Mechanochromic Switching between Delayed Fluorescence and Phosphorescence of Luminescent Coordination Polymers Composed of Dinuclear Copper(I) Iodide Rhombic Cores

Atsushi Kobayashi,*[a] Yuya Yoshida,[a] Masaki Yoshida,[a] and Masako Kato*[a]

Abstract: The synthesis and photophysical properties of two luminescent Cu(I) coordination polymers, $[Cu_2I_2(PPh_3)_2(3\text{-tpyb})]_n$ and $[Cu_2I_2(PPh_3)_2(4\text{-tpyb})]_n$ (**Cu-3-tpyb** and **Cu-4-tpyb**; PPh_3 = triphenylphosphine, *m*-tpyb = 1,3,5-tris(*m*-pyridyl)benzene (*m* = 3, 4)), are described. X-ray structural analysis indicated that one-dimensional coordination chains comprising rhombic $\{Cu_2I_2(PPh_3)_2\}$ cores and *m*-tpyb bridging ligands were formed. Both **Cu-3-tpyb** and **Cu-4-tpyb** exhibited blue-to-yellow thermally activated delayed fluorescence (TADF) that originated from mixing of the metal-to-ligand and halide-to-ligand charge-transfer excited states and moderate emission quantum yields of 0.29 and 0.27, respectively, at 298 K. Further, mechanochromic luminescence was observed for both complexes. The emission lifetimes indicated that the origin of emission switched from TADF to phosphorescence, which was derived from the triplet cluster-centred (^{3}CC) emissive state generated by grinding-induced amorphization.

Introduction

Luminescent Cu(I) complexes have attracted considerable attention as promising alternative materials to luminescent noble metal complexes because of their characteristic d^{10} electronic configuration that eliminates the non-radiative decay pathway from the d–d excited state.[1-7] Recent extensive studies of luminescent Cu(I) complexes have led to the achievement of interesting photophysical properties such as extremely bright emission with ~100% quantum yield,[8-9] thermally activated delayed fluorescence (TADF),[10-16] and external-stimuli responsive luminescence.[17-28] One of the characteristic features of luminescent Cu(I) complexes is that various emissive states can contribute to their luminescence. The metal-to-ligand charge-transfer (MLCT) excited state is a well-known emissive state of not only Cu(I) complexes but also of other noble metal complexes such as those of Ru(II), Ir(III), and Pt(II).[29-30] It is well known that in order for the Cu(I) complex to achieve high emission quantum yield, the Jahn-Teller flattening distortion of the MLCT excited state should be suppressed.[31-38] The wide emission color tuning ranging from blue to red has been also achieved by the modification of the π^* orbitals of the organic ligands.[39-41] Since the photoexcited electron and the remaining hole are spatially separated in the π^* orbital of the organic ligand and the 3d orbital of the Cu(I) ion, the energy gap between the single and triplet MLCT excited states tends to be small enough to permit an inverted intersystem crossing from the stable T_1 to relatively unstable S_1 state, resulting in TADF.[10-16] One of the other typical emissive states is the triplet cluster-centered (^{3}CC) excited state that is usually observed for the iodide-bridged Cu(I) cluster complexes.[42-45] An interesting feature is the external-stimuli responsive luminescence such as thermochromic, vapochromic, and mechanochromic luminescence that may be applicable to various types of sensors.[17-28] For example, interesting thermochromic luminescence has been observed for cubane-type Cu(I) cluster complexes $[Cu_4I_4(py)_4]$ and $[Cu_4I_4(PPh_3)_4]$ (py = pyridine, PPh_3 = triphenylphosphine).[18,20] Furthermore, mechanochromic luminescence has been reported for a similar cubane-type cluster complex, $[Cu_4I_4(PPh_2(CH_2CH{=}CH_2))_4]$, which has a slightly modified phosphine ligand.[21] An interesting phenomenon was recently reported by Farinella et al.; the coordination polymer $[Cu_2I_2(3\text{-pica})]_n$ (3-pica = 3-picolylamine) comprising the iodide-bridged rhombic $\{Cu_2I_2\}$ dinuclear cores and 3-pica linkers exhibited interesting thermochromic switching between TADF that was derived from the CT excited state and the phosphorescence originating from the ^{3}CC state.[27] However, the creation of such switching of the emission origins in the chromic behaviors in response to other external stimuli (e.g. vapors, mechanical grinding) is still a challenging research subject.

Recently, we have focused on the development of smart sensing functions based on the strongly emissive Cu(I) complexes. In this work, to switch the emission origin in the vapochromic and/or mechanochromic behavior, two different types of organic ligands were selected. One of these ligands is 1,3,5-tris(*m*-pyridyl)benzene (Scheme 1; *m*-tpyb, *m* = 3, 4),[46,47] which can adopt various coordination modes

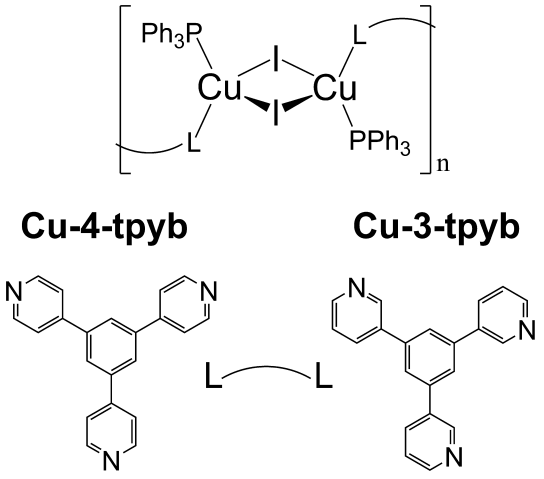

Scheme 1. Schematic molecular structures of coordination polymers, **Cu-4-tpyb** and **Cu-3-tpyb**.

[a] Dr. A. Kobayashi, Mr. Y. Yoshida, Dr. M. Yoshida, and Prof. M. Kato.
Department of Chemistry, Faculty of Science, Hokkaido University
North-10 West-8, Kita-ku, Sapporo 060-0810, Japan
E-mail:akoba@sci.hokudai.ac.jp (Dr. A. Kobayashi)
mkato@sci.hokudai.ac.jp (Prof. M. Kato)

Supporting information for this article is given via a link at the end of the document.

to bridge several Cu(I) ions based on the three pyridinyl N atoms. The other ligand is PPh_3, which is used to construct a sterically bulky coordination environment around the Cu(I) ion. Herein, the synthesis, crystal structures, and photophysical properties of the newly synthesized luminescent Cu(I) coordination polymers, $[Cu_2I_2(PPh_3)_2(m\text{-tpyb})]_n$ (m = 3,4; hereafter **Cu-m-tpyb**), have been described. Furthermore, it has been demonstrated that both **Cu-m-tpyb** exhibited strong TADF with CT character and an interesting mechanochromic behavior involving the switching of the emission origin from TADF to ^{3}CC phosphorescence from the impurity sites generated during the grinding-induced amorphization.

Results and Discussion

Crystal structures

Figure 1 shows the crystal structure of **Cu-4-tpyb**. Crystallographic data and the selected bond lengths and angles are listed in Tables S1 and S2. **Cu-4-tpyb** consisted of two crystallographically independent Cu ions, two iodide anions, two PPh_3 ligands, and a 4-tpyb bridging ligand. Each Cu ion adopted a typical tetrahedral coordination geometry for Cu(I) ion, where the Cu^+ ion was surrounded by two I^- ions, the P atom of PPh_3, and the N atom of 4-tpyb. The two Cu^+ ions were bridged by two I^- ions to form a $\{Cu_2I_2\}$ rhombic core. The Cu–N bond distances in **Cu-4-tpyb** ranged from 2.071(8) to 2.081(8) Å and the two Cu–P bond distances were 2.218(3) Å. These distances were comparable to the other halide-bridged Cu(I) complexes with *N*-heteroaromatic ligands and PPh_3.[39] The Cu···Cu distance in the $\{Cu_2I_2\}$ core (3.302(2) Å) was longer than the sum of the van der Waals radii of Cu (2.8 Å) and indicated negligible metallophilic interactions. Two of the three N atoms of the 4-tpyb ligand were coordinated to two different $\{Cu_2I_2\}$ cores to form a spiral one-dimensional (1-D) chain structure along the *a* axis (see Figure 1a). The non-coordinating N atom of 4-tpyb ligand could form a weak hydrogen bond with the H atom of the central benzene ring of the 4-tpyb ligand of the adjacent 1-D chain, which connected the 1-D chains along the *b* axis (C-H···N = 3.605 Å, Figure S1). As shown in Figure 1b, there were four porous channels in one unit cell along the *b* axis in which two $CHCl_3$ and a H_2O molecule were adsorbed. The diameter and void fraction were estimated to be 5.8 Å×8.5 Å and 20%, respectively. There were no remarkable interactions between the adsorbed solvent molecules and the coordination-polymer framework.

The crystal structure of **Cu-3-tpyb** is depicted in Figure 2. A similar 1-D chain structure to that of **Cu-4-tpyb** was also confirmed in **Cu-3-tpyb**, wherein the 3-tpyb ligands bridged the rhombic dinuclear cores along the *c* axis (Figure 2a). The Cu–N and Cu–P bonds distances were similar to those of **Cu-4-tpyb** (Table S2). A noticeable difference between these **Cu-m-tpyb** coordination polymers is the number of crystallographically independent dinuclear cores in the unit cell; two independent cores were found in **Cu-3-tpyb**. The Cu···Cu distance in the $\{Cu(1)_2–I(1)_2\}$ core (2.9530(7) Å) was shorter by about 0.4 Å than the that in the $\{Cu(2)_2\text{-}I(2)_2\}$ core (3.3569(7) Å). However,

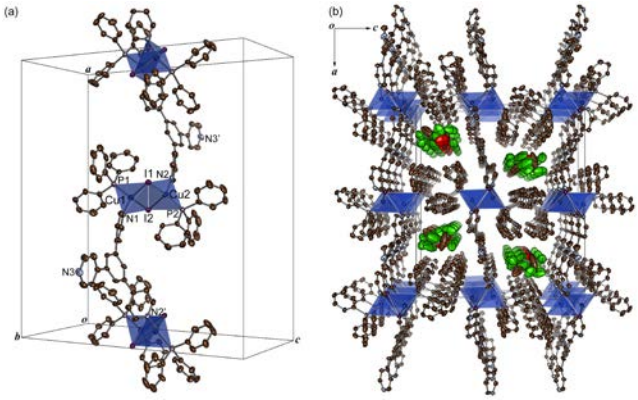

Figure 1. Crystal structure of **Cu-4-tpyb**. (a) 1-D coordination chain structure and (b) packing diagram viewed along the *b* axis. Coordination spheres of Cu(I) ions are shown as blue tetrahedrons. Brown, light blue, red, green, and purple ellipsoids represent C, N, O, Cl, and I atoms, respectively. All H atoms are omitted for clarity.

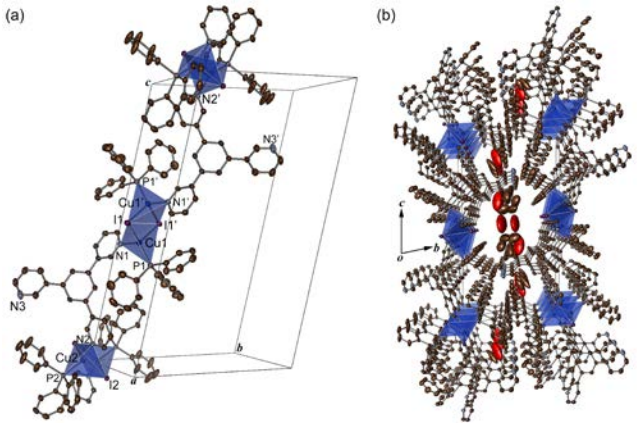

Figure 2. Crystal structure of **Cu-3-tpyb**. (a) 1-D coordination chain structure and (b) packing diagram viewed along the *a* axis. Coordination spheres of Cu(I) ions are shown as blue tetrahedrons. Brown, light blue, red, and purple ellipsoids represent C, N, O, and I atoms, respectively. All H atoms are omitted for clarity.

both distances were longer than the sum of the van der Waals radii of Cu (2.8 Å), and the metallophilic interactions in these dinuclear cores were also negligible. Similar to the 4-tpyb ligands of **Cu-4-tpyb**, two of the three N atoms of the 3-tpyb ligand were coordinated to the Cu^+ ions and the remaining one formed a weak hydrogen bond with the H atom of one of the phenyl rings of PPh_3 of the adjacent 1-D chain (C-H···N = 3.320 Å). There were two different porous channels along the *a* axis as shown in Figure 2b. One THF and one water molecule per $\{Cu_2I_2\}$ core were found in the larger pore channel, which had a diameter of 6.7 Å×6.9 Å. In the smaller pore with the diameter 5.8 Å×3.6 Å, only one THF molecule per one $\{Cu_2I_2\}$ core was found (Figure 2b). As a result, a slightly larger accessible void (~27 % in the unit cell) than **Cu-4-tpyb** was formed. There were no significant interactions between the solvent molecules in the pores and the porous framework as in the case of **Cu-4-tpyb**.

Photophysical properties

Figures 3(a) and 3(b) show the emission spectra of solid-state **Cu-4-tpyb** and **Cu-3-tpyb** at 298 and 78 K. The purity of each sample was checked by powder X-ray diffraction (PXRD) patterns and elemental analysis (see Figure S2 and experimental section). **Cu-4-tpyb** exhibited a broad emission band centered at 545 nm at 298 K and this band was shifted to longer wavelengths by up to 570 nm when the temperature was reduced to 78 K. A similar broad emission band at 498 nm was observed for **Cu-3-tpyb** at 298 K, while the emission spectrum at 78 K was composed of two emission bands; one is the broad band centered at 545 nm and another corresponds to the higher-energy bands with vibrational progression at 442 nm. This difference suggests that the emission origin of **Cu-3-tpyb** changed when the temperature was decreased. Since the isomorphous structure of **Cu-3-tpyb** to that of 150 K was clearly identified at 97 K (Table S1), the observed change in emission spectrum would not be due to the solid-state transition, but due to the change of the emission origin. The wavelength difference between the emission maxima of **Cu-m-tpyb** (m = 3, 4) of ~47 nm suggests that the position of the coordinating N atoms in the tpyb ligand is an important factor for the emission energy. The similar luminescent Cu(I) coordination polymer, $[Cu_2I_2(PPh_3)_2(4,4'\text{-bpy})]_n$, reportedly exhibited emission maxima at 542 nm,[39] which is comparable to that of **Cu-4-tpyb**.

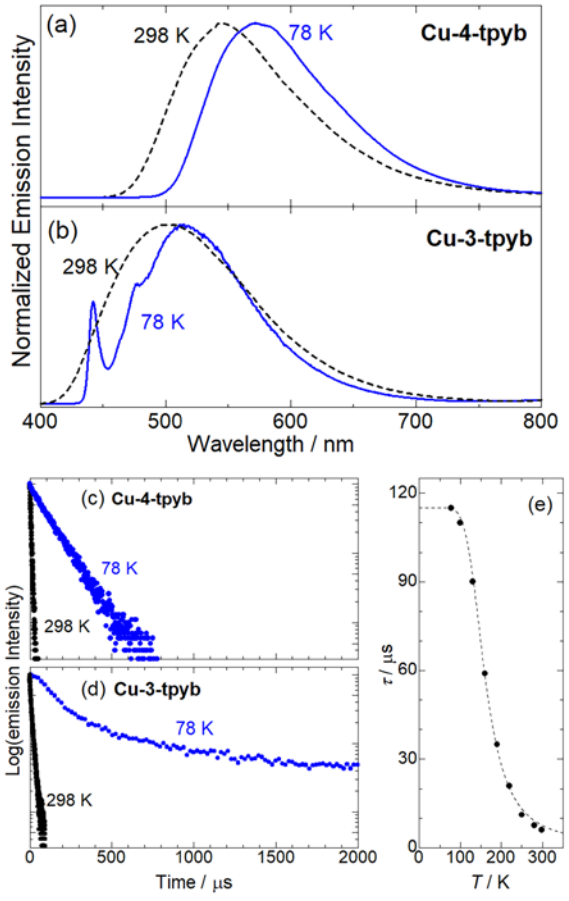

Figure 3. Temperature dependencies of the emission spectra of (a) **Cu-4-tpyb** and (b) **Cu-3-tpyb** at 298 K (black dotted line) and 78 K (blue solid line) in the solid state (λ_{ex} = 350 nm). Emission decays of (c) **Cu-4-tpyb** and (d) **Cu-3-tpyb** at 298 K (black circles) and 78 K (blue circles) in the solid state (λ_{ex} = 337 nm). (e) Temperature dependence of the emission lifetime of **Cu-4-tpyb** in the solid state. The dotted line was calculated using eq. (1).

Table 1. Luminescence properties of **Cu-4-tpyb** and **Cu-3-tpyb** in the solid states at 298 and 77 K.

Complex	**Cu-4-tpyb**				**Cu-3-tpyb**			
	As synthesized		Ground		As synthesized		Ground	
T (K)	298	78	298	78	298	78	298	78
λ_{max} [a] (nm)	545	570	605	605	498	442, 477, 510	553	445, 543
τ (μs)	6.04	115	0.447, 1.340, 3.181	6.28, 23.6, 108	4.78, 14.47	155, 625, 3513	1.012, 3.957, 9.148	49.0, 123, 690
τ_{av} (μs)	-	-	2.27	66.1	12.46	1879	6.62	529.9
Φ_{em}	0.29	0.84	0.10	0.36	0.27	0.73	0.30	0.67
k_r (s^{-1}) [b]	4.80×10^4	1.11×10^3	4.40×10^4	5.51×10^3	2.17×10^4	3.88×10^2	4.53×10^4	1.26×10^3
k_{nr}(s^{-1}) [c]	1.17×10^5	3.71×10^2	3.96×10^5	9.80×10^3	5.86×10^4	1.44×10^2	1.06×10^5	6.23×10^3

[a] Emission maximum. [b] Radiative rate constants, k_r, were estimated by Φ_{em}/τ. [c] Nonradiative rate constants, k_{nr}, were estimated by $k_r(1-\Phi_{em})/\Phi_{em}$.

To elucidate the emission behaviors of **Cu-m-tpyb** in detail, their emission lifetimes and quantum yields were measured in the solid state at both 298 and 78 K. The results are summarized in Table 1. As shown in Figure 3(c), a single exponential decay was observed in the emission decay curve of **Cu-4-tpyb** at both temperatures and the lifetime was estimated to become longer from 6.04 μs at 298 K to 115 μs at 78 K, which are comparable values to that of $[Cu_2I_2(PPh_3)_2(4,4'\text{-bpy})]_n$ (τ = 4.0 μs at 298 K, 67 μs at 80 K).[39] Such significant increase in the emission lifetime has been previously reported for the thermally activated delayed-fluorescent (TADF) Cu(I) complexes.[12,13,41] For example, Tsuboyama et al. reported that the Cu(I) dimer complex, $[Cu_2I_2$(2,3-bis(diphenylphosphyno)benzene)$_2]$, exhibited an increase in the emission decay on the scale of two orders of magnitude from 4.0 μs at 298 K to 211 μs at 77 K.[12] In contrast, smaller temperature dependence of the emission lifetime has been reported for the halide-bridged Cu(I) cluster complexes, one of the typical materials showing triplet cluster-centered (^{3}CC) emission.[18,20,26] For example, the emission lifetimes of the cubane-type cluster complexes, $[Cu_4I_4(py)_4]$ and

$[Cu_4I_4(PPh_3)_4]$, increased by less than one order of magnitude from 11 and 4.7 μs at 298 K to 25.5 and 26 μs at 77 K, respectively.[18,20] The large temperature dependence of the emission lifetime and the broad spectral shape without vibrational progression of **Cu-4-tpyb** suggest that the origin of emission could be ascribed to TADF from the charge-transfer excited state. In fact, the radiative decay constant (k_r) estimated from the emission lifetime and the emission quantum yield decreased remarkably to one fiftieth upon decreasing the temperature (see Table 1).

Further investigation of the origins of emission from **Cu-4-tpyb** was conducted by measuring the emission lifetime at various temperatures and the results are shown in Figure 3(e). Assuming the two-state model involving the lowest excited singlet state (S_1) and the lowest excited triplet state (T_1), the observed lifetime (τ) can be expressed as a Boltzmann average by using equation (1).[48]

$$\tau = \frac{3+exp(-\Delta E/RT)}{3/\tau_{T_1}+1/\tau_{S_1}exp(-\Delta E/RT)} \quad (1)$$

where, Δ*E* is the energy difference between the singlet and triplet states, τ_{S1} and τ_{T1} are the lifetimes of S_1 (fluorescence) and T_1 (phosphorescence) states, respectively, *R* is the ideal gas constant, and *T* is the absolute temperature. The corresponding fitting result based on equation (1) for the temperature dependence of the observed emission lifetime is shown as the dotted line in Figure 3(e). The obtained Δ*E* value (650 cm^{-1}) was comparable to the difference in the wavelengths of emission maxima at 298 and 78 K (805 cm^{-1}). These results clearly indicate that the emission of **Cu-4-tpyb** was attributable to TADF originating from the CT excited state.

As shown in Figure 3(d), a double exponential decay was observed for **Cu-3-tpyb** at 298 K and the estimated emission lifetimes were 4.78 and 14.47 μs. Considering that there are two crystallographically different $\{Cu_2I_2\}$ cores in the crystal structure of **Cu-3-tpyb**, these two emission components may be derived from these two different cores with the same emissive state. At 78 K, three emission components with lifetimes of 155 μs, 625 μs, and 3.51 ms were observed. These lifetimes are remarkably longer than the emission lifetime of **Cu-4-tpyb**, implying the contribution of a different emissive state. Since the emission band with clear vibrational progression was observed at 78 K (Figure 3(b)), one plausible origin is the triplet ligand-centered ($^3\pi$–π) excited state. In the time-resolved emission spectra of **Cu-3-tpyb** at 78 K, only the broad emission band centered at ~500 nm was observed before 1.5 ms, but another sharp peak at 450 nm that was probably derived from the $^3\pi$–π state was clearly observed over a longer time range (>2 ms). Thus, the longest emission component of **Cu-3-tpyb** could be attributed to the $^3\pi$–π emission of the bridging 3-tpyb ligand. The other two shorter-lived emission components were ascribed to TADF from the CT excited state like **Cu-4-tpyb**, because the average emission lifetimes of these two components (τ_{av} = 12.5 and 155 μs at 298 and 78 K, respectively) were comparable to that of **Cu-4-tpyb**. It is worth noting that only **Cu-3-tpyb** exhibited the ligand-centered $^3\pi$–π emission, which was because of its higher-energy CT state compared to that of **Cu-4-tpyb** (as evidenced by the higher energy emission of **Cu-3-tpyb** by ~45 nm at 298 K. In other words, the rapid radiative decay process *via* TADF was the dominant pathway at 298 K because of the spin-allowed fluorescence character of the S_1 state, while it was strongly prohibited at a lower temperature of 78 K. A slower radiative decay process was observed from the thermally accessible $^3\pi$–π state.

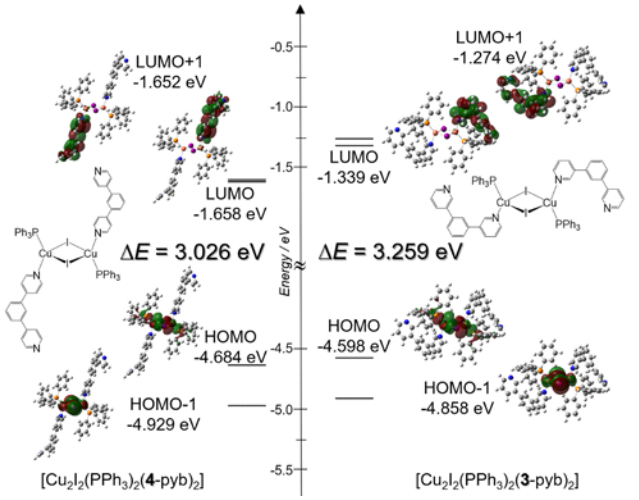

Figure 4. Schematic molecular orbital diagrams for the model dinuclear complexes, (left) $[Cu_2I_2(PPh_3)_2(4\text{-pyb})_2]$ and (right) $[Cu_2I_2(PPh_3)_2(3\text{-pyb})_2]$. The energy gap between HOMO and LUMO is also shown.

To further investigate the emission origins of the **Cu-m-tpyb** (m = 3, 4) coordination polymers, DFT calculations were conducted for the simplified Cu(I) dinuclear complexes, $[Cu_2I_2(PPh_3)_2(m\text{-pyb})_2]$ (*m* = 3, 4, *m*-pyb = 1,3-(*m*-pyridyl)benzene). Schematic molecular orbital diagrams of the ground states are shown in Figure 4. The structure optimizations were started from the X-ray structures by replacing the pyridyl group of the *m*-tpyb ligand coordinating to the adjacent Cu_2I_2 core by an H atom. In both simplified dinuclear complexes, the highest-occupied molecular orbital (HOMO) and HOMO-1 comprised the 3d orbitals of the two Cu(I) ions and the 5p orbitals of two iodide ions, while the lowest-unoccupied molecular orbital (LUMO) and LUMO+1 were delocalized on the π* orbital of the *m*-pyb ligand. The energy difference between the HOMO and LUMO of $[Cu_2I_2(PPh_3)_2(4\text{-pyb})_2]$ was larger (by ~0.2 eV) compared to that of $[Cu_2I_2(PPh_3)_2(3\text{-pyb})_2]$. Since this difference estimated by DFT calculations was qualitatively matched with the difference of emission energy between **Cu-4-tpyb** and **Cu-3-tpyb**, the emission of **Cu-m-tpyb** could be originated from the metal-to-ligand charge-transfer state effectively mixed with the halide-to-ligand charge-transfer ((M+X)LCT) state. Accordingly, the higher-lying π* orbital of 3-tpyb as compared to that of 4-tpyb was the origin of the shorter wavelength emission of **Cu-3-tpyb** than that of **Cu-4-tpyb**. Our DFT calculations also suggested that the ^{3}CC excited state with an effective Cu–Cu interaction was hardly accessible; the LUMO with the bonding character between the two Cu(I) ion in the rhombic core was found at

LUMO+27 and the energy difference from LUMO was above 2.6 eV (see Figures S3 and S4). This is consistent with the X-ray structures that showed longer Cu···Cu distances in the core (more than twice of the van der Waals radius of Cu, as described in the section discussing crystal structures. We also checked the contribution of the ligand-centered π–π* transition from the ground state MO diagrams. The highest-occupied π orbital of the *m*-pyb ligand was found at HOMO-12 in $[Cu_2I_2(PPh_3)_2(3\text{-pyb})_2]$, but the corresponding orbital of $[Cu_2I_2(PPh_3)_2(4\text{-pyb})_2]$ was found at the more stable HOMO-19. The energy difference between these MOs and HOMOs was also smaller in $[Cu_2I_2(PPh_3)_2(3\text{-pyb})_2]$ (1.78 eV) than that in $[Cu_2I_2(PPh_3)_2(4\text{-pyb})_2]$ (2.10 eV). This result was experimentally supported by the UV-Vis absorption spectra of the *m*-tpyb ligands; the lowest absorption band of 3-tpyb was shifted to shorter wavelengths by about 15 nm compared to that of 4-tpyb in the $CHCl_3$ solutions (Figure S5). Thus, the ^{3}π–π* excited state of **Cu-3-tpyb** was likely more stable and accessible than that of **Cu-4-tpyb**, resulting in the observation of ^{3}π–π* emission with a clear vibrational progression at 78 K.

Mechanochromic luminescence

As discussed previously, solvated $CHCl_3$ and water molecules were present in the porous channels of **Cu-4-tpyb**, suggesting the possibility of luminescence chromism based on the adsorption/desorption of these guest molecules. Thus, we investigated the changes in the emission spectra under various conditions. As shown in Figure 5(a), the emission spectrum of as-synthesized **Cu-4-tpyb** was hardly changed upon removal of the solvated $CHCl_3$ and water molecules under vacuum (black and red curves in Figure 5(a)). Photographs of the crystalline samples of **Cu-4-tpyb** under bright field and UV light irradiation were also negligibly changed in this drying process (Figure 5(c) and 5(d)). Notably, the emission spectrum and photographs were remarkably changed by manually grinding the dried sample

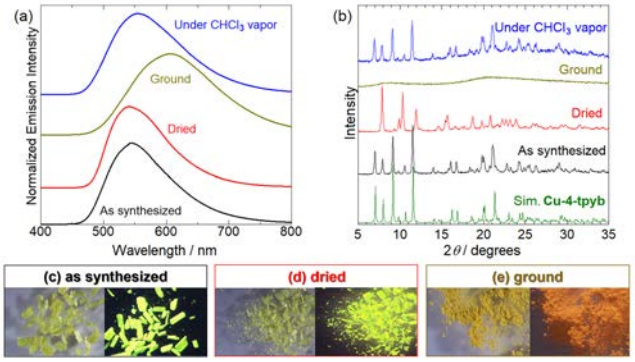

Figure 5. Changes in the (a) emission spectrum (λ_{ex} =350 nm) and (b) PXRD pattern of **Cu-4-tpyb** upon drying under vacuum (red), subsequent manual grinding in a mortar (brown), and exposure to $CHCl_3$ vapor at room temperature (blue). Black lines in both panels show the spectrum and patterns of the as-synthesized **Cu-4-tpyb**. The green curve in (b) is the simulation pattern calculated based on the X-ray structure of **Cu-4-tpyb**. Photographs in (left) bright field and (right) under UV light of (c) as synthesized, (d) vacuum-dried and (e) ground **Cu-4-tpyb** are shown.

in a mortar; the emission maximum was observed at 605 nm and the color under bright field was changed from clear yellow to brown after grinding (brown curve in Figure 5(a) and 5(e)). Further, the original emission spectrum with the maximum at 545 nm was recovered by exposing the ground sample to $CHCl_3$ vapor in air (blue curve in Figure 5(a)). These results indicate that **Cu-4-tpyb** exhibits mechanochromic luminescence upon manual grinding and exposure to $CHCl_3$ vapor. Similar spectral changes were observed in the excitation and UV-Vis diffuse reflectance spectra (see Figure S6), suggesting that the mechanochromic behavior likely originated from the structural transformation in the ground state and not structural relaxation in the excited state.

To elucidate the mechanism of the mechanochromic luminescence of **Cu-4-tpyb**, PXRD patterns of these four different samples were measured. As shown in Figure 5(b), as-synthesized **Cu-4-tpyb** exhibited an almost identical pattern to the simulation calculated from the X-ray structure, while the diffraction pattern of the dried sample was completely different to that of the as-synthesized sample. Considering the thermogravimetric analysis (TGA) results showing that all solvated $CHCl_3$ and water molecules were removed under vacuum (see Figure S7), the change in the PXRD pattern indicates that the porous structure of **Cu-4-tpyb** could not be retained without the solvated guest molecules in the pores. On the other hand, the almost identical emission spectra of the as-synthesized and dried samples suggest that the collapse of the porous structure hardly affected the (M+X)LCT transition energy of **Cu-4-tpyb**. In contrast, no sharp peak was observed in the PXRD pattern of the ground sample, indicating that grinding induced amorphization. The remarkable changes in color and emission upon grinding suggest that amorphization influences the structure around the $\{Cu_2I_2\}$ core. After exposing the ground sample to $CHCl_3$ vapors in air, an almost identical PXRD pattern to that of the as-synthesized sample was observed. These changes in the PXRD experiments clearly revealed that the reversible crystal-to-amorphous transformation was the origin of mechanochromic luminescence of **Cu-4-tpyb**.

Since the remarkable color and luminescence changes and the mechanochromic behavior of **Cu-4-tpyb** suggested a change in the origin of luminescence, the emission lifetime and quantum yield of the ground sample were determined at 298 and 78 K. The observed emission decay curves of ground **Cu-4-tpyb** at 298 and 78 K are shown in Figures 6(a) and 6(b), respectively, and compared with that of the as-synthesized sample (the same data shown in Figure 3(c)). The results and estimated k_r and non-radiative decay constant (k_{nr}) are listed in Table 1. The emission quantum yield decreased to one third of the as-synthesized sample at both temperatures upon manual grinding. Although the emission lifetime of the ground sample was also estimated to decrease to one-third, the observed emission decay curve could be fitted by at least triple exponentials (τ_1, τ_2, and τ_3) at both 298 and 78 K. Considering that a single exponential decay was observed in the emission decay of the as-synthesized **Cu-4-tpyb**, different emissive state(s) may be generated in the ground sample. Further investigation of the origin of emission for the ground sample was conducted by

variable-temperature emission lifetime experiments (Figures 6(c) and 6(d)). In this low temperature range, three different emission components were commonly observed, and the main contribution was that of the middle lifetime component τ_2; the component fraction of τ_2 was constantly over 50% in this temperature range (see Figure 6(c)). The temperature dependence of the longest-lived emission component (τ_3) qualitatively in agreement with that of the as-synthesized sample and successfully fitted by equation (1) (blue dotted curve in Figure 6(c)), suggesting the existence of the same TADF emission species with the ^{3}(M+X)LCT character. However, the component fraction was less than 25% at all measured temperatures. In contrast, the two shorter-lived emission species (τ_1 and τ_2) exhibited completely different temperature dependence to that of the τ_3 component; the smaller temperature dependences of the emission lifetimes ranging from 0.44 to 23 μs clearly indicated the contribution of the other emission species. It should be noted that a comparable emission lifetime was observed for several cubane-type Cu(I) cluster complexes (e.g., $[Cu_4I_4(PPh_3)_4]$), which showed that phosphorescence originated from the ^{3}CC excited state as mentioned above.[18,20] Although the structure of ground **Cu-4-tpyb** was still unclear owing to its amorphous nature, it was possible for the ground **Cu-4-tpyb** to form the cubane-type $\{Cu_4I_4\}$ cluster, which is the typical structure for ^{3}CC emissive complexes, because the moderate void fraction in the unit cell (~20%) likely allowed the drastic structural transformation from the rhombic-type $\{Cu_2I_2\}$ core to the cubane-type $\{Cu_4I_4\}$ core. Thus, the temperature dependence of the emission lifetime of ground **Cu-4-tpyb** suggests that the mechanochromic luminescence of **Cu-4-tpyb** involves a unique switching of the emission origin between TADF from the (M+X)LCT excited state and phosphorescence derived from the ^{3}CC excited state.

We also investigated the mechanochromic behavior of **Cu-3-tpyb** because this coordination polymer has similar porous channels and 1-D coordination chains as that of **Cu-4-tpyb**.

Figures 7(a) and 7(b) display the changes in the emission spectrum and PXRD pattern of **Cu-3-tpyb** under various conditions. The as-synthesized sample exhibited light blue emission (Figure 7(c)) with the maximum at 498 nm and the PXRD pattern was identical to the one simulated based on the X-ray structure. Although the emission spectrum of **Cu-4-tpyb** hardly showed any change upon drying under vacuum as discussed above, the luminescence color of **Cu-3-tpyb** turned bluish-green as shown in Figure 7(d) upon vacuum-drying and the emission maximum was red-shifted by about 17 nm. Furthermore, the intensity of the strongest (010) diffraction peak of the as-synthesized sample observed at 6.6° decreased significantly and most peaks shifted to higher angles. Additional changes in the emission spectrum and PXRD pattern were observed upon drying for the second time by heating to 120 °C; the luminescence color was changed to light green (Figure 7(e)) and the wavelength of emission maximum was red-shifted to 545 nm. The strongest diffraction peak in the PXRD pattern was also shifted to a higher angle (7.6°). These results suggest that the solvated THF molecules in **Cu-3-tpyb** were removed in two steps. In fact, TG analyses of these two dried samples under vacuum at room temperature and at 120 °C in air clearly indicate that one of the two solvated THF molecules could be removed by drying under vacuum whereas all solvated THF and water molecules were removed by heated drying (see Figure S8). This result is reasonable because there are two different porous channels in the crystal structure of **Cu-3-tpyb**; one of the two channels was occupied by only THF and the other was filled by THF and water molecules (Figure 2(b)). Thus, these changes observed in the emission spectrum may be attributed to the removal of solvated molecules from the porous structure of **Cu-3-tpyb**, which involves significant changes in the crystal structure. Interestingly, the emission color was changed to greenish-yellow upon manual grinding of all the three states (Figure 7(f)). Same as **Cu-4-tpyb**, the PXRD pattern of ground **Cu-3-tpyb** exhibited a featureless broad pattern, indicating

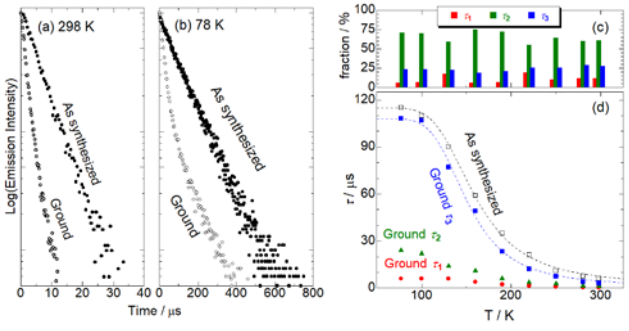

Figure 6. Emission decays of the as-synthesized (closed circles) and ground samples (open circles) of **Cu-4-tpyb** at (a) 298 K and (b) 78 K in the solid state (λ_{ex} = 337 nm). Temperature dependence of (c) the fraction and (d) lifetime of each emission component (red, green, and blue symbols represent the emission components with short (τ_1), middle (τ_2), and long (τ_3) lifetimes) observed for the ground sample of **Cu-4-tpyb**. Data of the as-synthesized **Cu-4-tpyb** is also shown in (d).

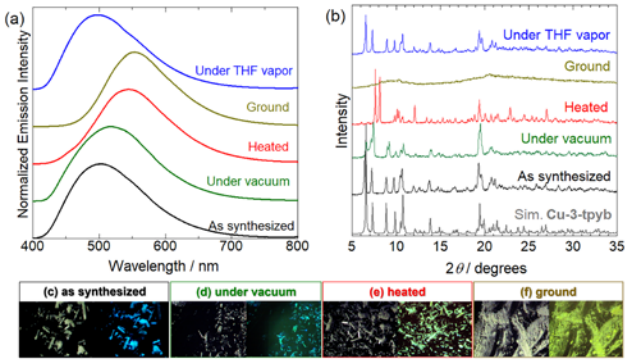

Figure 7. Changes in the (a) emission spectrum (λ_{ex} =350 nm) and (b) PXRD pattern of **Cu-3-tpyb** by (green) drying under vacuum, and subsequent (red) heating, (orange) manual grinding, and (blue) exposure to THF vapor at room temperature. Black curves show the spectrum and pattern of the as-synthesized sample. Gray curve at the bottom in (b) shows the simulation pattern calculated from the crystal structure of **Cu-3-tpyb**. Photographs in (left) bright field and (right) under UV light of the (c) as-synthesized, (d) vacuum-dried, (e) heat-dried, and (d) ground **Cu-3-tpyb** are shown.

amorphization as a result of manual grinding. The original light blue emission and almost identical PXRD pattern to the simulation based on the X-ray structure of **Cu-3-tpyb** were recovered by exposing these dried and/or ground samples to THF vapor in air. These changes observed in the emission spectrum and PXRD pattern clearly indicate that **Cu-3-tpyb** exhibits reversible luminescent vapochromism and mechanochromism. To elucidate the emission origin of the ground **Cu-3-tpyb**, the emission decay and quantum yield were evaluated. Obtained results and estimated k_r and k_{nr} values are summarized in Table 1. Interestingly, the emission quantum yield of ground **Cu-3-tpyb** was comparable (Φ = 0.30 at 298 K and 0.67 at 78 K) to that of the as-synthesized sample whereas the emission lifetime of the ground sample was remarkably shorter by about half of the as-synthesized sample at both 298 and 78 K (Figure S9). Estimated k_r value of the ground state was remarkably higher by about two and three times than that of the as-synthesized sample, indicating the contribution of the different emissive states. As discussed before, the emission of the as-synthesized **Cu-3-tpyb** could be attributed to TADF that derived from the (M+X)LCT emissive state at ~298 K in addition to the phosphorescence from the ligand-centered π–π* excited state at 78 K. On the other hand, sharp peaks characteristic of $^3\pi$–π* emission were hardly observed for the ground sample in the time-resolved emission spectrum at 78 K (see Figure S10). Thus, the (M+X)LCT emissive state was stabilized by grinding-induced amorphization than the $^3\pi$–π* state. Since the triple exponential decay was observed even for the as-synthesized crystal of **Cu-3-tpyb**, the assignment for each emission component observed for the ground sample is difficult. However, the emission lifetime of the shortest-lived component was in the same time range as that of the emission assigned to the ^{3}CC transition of ground **Cu-4-tpyb**, suggesting that the ^{3}CC excited state contributed to the emission properties of ground **Cu-3-tpyb** as well as **Cu-4-tpyb**.

Plausible mechanism of mechanochromic luminescence

As mentioned previously, both **Cu-m-tpyb** (m = 3, 4) exhibited a unique mechanochromic luminescence involving switching between TADF and phosphorescence. In this section, we discuss a plausible mechanism of this switching behavior. Scheme 2 shows the schematic energy diagrams of both the as-synthesized and ground samples of **Cu-4-tpyb**. As indicated by X-ray structures and DFT calculations for the simplified dinuclear complexes $[Cu_2I_2(PPh_3)_2(m\text{-pyb})_2]$, the metallophilic interactions between the two Cu(I) ions in the rhombic core were negligible for both **Cu-m-tpyb**. Thus, ^{3}CC emission was hardly observed for the as-synthesized samples. DFT calculations also suggested that the HOMO and LUMO were localized on the rhombic $\{Cu_2I_2\}$ core and the pyb ligand (see Figure 4). This specially separated electronic structure should contribute to the small energy gap between the singlet and triplet (M+X)LCT excited state. Consequently, TADF originating from the(M+X)LCT excited state was observed for both **Cu-m-tpyb** (m = 3, 4) (Scheme 2(a)). This is consistent with the small energy gap (ΔE = 650 cm^{-1}) estimated by the temperature

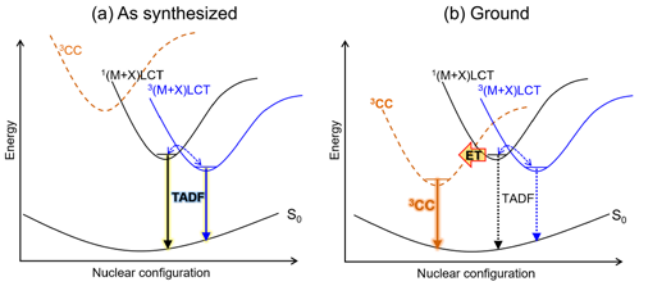

Scheme 2. Schematic energy diagrams of the (a) as-synthesized and (b) ground samples of **Cu-4-tpyb**.

dependence of emission lifetimes (see Figure 3(e)). On the other hand, the structure of the ground samples of **Cu-m-tpyb** is still unclear because of their amorphous nature, although an almost identical IR spectrum to that of the dried samples was observed (Figure S11), which suggested that 1-D coordination chain structures would be retained after grinding-induced amorphization, even though the range of the structural ordering should be shorter than that in the as-synthesized sample. Considering that the weak lower-energy absorption and excitation bands appeared on grinding (Figure S6), it is reasonable to expect that some defects and/or impurity sites would be formed. One plausible origin of such an impurity site might be the cubane-type $\{Cu_4I_4\}$ cores that could be formed upon breaking of 1-D coordination chains and the following dimerization of the coordinatively unsaturated $\{Cu_2I_2\}$ dimers at the terminals. Plausibly, the lower-energy ^{3}CC emission was observed as the dominant component for the ground samples because of a Dexter-type energy transfer from the higher-energy (M+X)LCT excited states through the 1-D coordination chains (i.e., energy migration). Such emission via energy migration through 1-D coordination chains has been previously reported by Tsuge et al.; the Cu(I)–Ag(I) mixed metal luminescent coordination polymer, $[Ag_{2-x}Cu_xI_2(PPh_3)_2(bpy)]_n$, exhibited emissions that originated from the Cu(I) site as the dominant species even in the extremely low Cu(I) dopant concentration (x = 0.005).[49] Thus, in the emission of ground samples of **Cu-m-tpyb** (m = 3, 4), the (M+X)LCT excitons generated in the 1-D coordination chains could migrate and get captured by the impurity site with the lower-energy ^{3}CC emissive state. In fact, the mechanochromic switching behavior of **Cu-4-tpyb** strongly depended on the degree of manual grinding; the lightly ground sample exhibited a long emission lifetime comparable to that of the as-synthesized sample (Figure S12), implying that the breaking of 1-D coordination chains by manual grinding is an important step to generate the lower-energy ^{3}CC emissive state. In the case of **Cu-3-tpyb**, the mechanochromic behavior was more complicated than that of **Cu-4-tpyb** because of the contribution of the ligand-centered $^3\pi$–π emissive state. However, the shorter Cu(I)···Cu(I) distance in the rhombic $\{Cu_2I_2\}$ core and the larger void fraction of **Cu-3-tpyb** compared to those in **Cu-4-tpyb** (Table S2) implied that the cubane-type $\{Cu_4I_4\}$ structure was easily formed as the impurity site during the grinding-induced amorphization process. Therefore, we believe that the

emission origin of **Cu-3-tpyb** was switched between TADF and phosphorescence in the mechanochromic luminescence behavior.

Conclusions

Two new luminescent Cu(I) coordination polymers **Cu-m-tpyb**, formulated as $[Cu_2I_2(PPh_3)_2(m\text{-tpyb})]_n$, were synthesized. X-ray diffraction study revealed that 1-D coordination chains comprising rhombic $\{Cu_2I_2(PPh_3)_2\}$ cores and the bridging *m*-tpyb ligands were commonly formed in both complexes and solvated guest molecules existed in between the chains. Both **Cu-m-tpyb** (m = 3, 4) exhibited interesting TADF that was derived from the singlet and triplet (M+X)LCT excited states as suggested by the temperature dependence of the emission lifetime and DFT calculations, which were based on the simplified dinuclear Cu(I) complexes, $[Cu_2I_2(PPh_3)_2(m\text{-pyb})_2]$. Although the luminescence color of **Cu-4-tpyb** was hardly changed by the removal of the solvated guest molecules, remarkable mechanochromic luminescence was observed by manual grinding and exposure to $CHCl_3$ vapor. In contrast, interesting vapochromic luminescence was observed in addition to the similar mechanochromic luminescence of **Cu-4-tpyb** for **Cu-3-tpyb** in response to the adsorption/desorption of the solvated THF molecules. The unique mechanochromic switching between TADF derived from the (M+X)LCT excited states and phosphorescence, which originated from the ^{3}CC state, was suggested by the temperature dependence of the emission lifetime of the ground samples. A plausible mechanism is the energy transfer from the (M+X)LCT excited state to the lower-energy ^{3}CC emissive state of the impurity sites that were generated by the grinding-induced amorphization of **Cu-m-tpyb**. Further studies of the switching of emission origin as a result of various external stimuli is now in progress.

Experimental Section

Synthesis

Organic bridging ligands, 4-tpyb and 3-tpyb, were prepared according to the literature procedure.[46,47] Copper iodide was purchased from Wako Pure Chemical Industries, Ltd. Triphenylphosphine (PPh_3) and solvents used in this work were purchased from Kanto Chemical Co. Inc. All reagents were used as received.

Synthesis of $[Cu_2I_2(4\text{-tpyb})_2(PPh_3)_2]_n$ (Cu-4-tpyb)

CuI (19.1 mg, 100 μmol) was added to a solution of PPh_3 (55.2 mg, 210 μmol) in a mixture of MeOH (1 mL) and $CHCl_3$ (2 mL). After stirring for 15 min at room temperature, the bridging ligand, 4-tpyb (15.2 mg, 48.2 μmol) was added and the reaction mixture was stirred for another 5 min at room temperature. Subsequently, the mixture was filtered to remove the unreacted insoluble materials. After standing the filtrate for several days at 30 °C, yellow crystals were collected by filtration and washed using a small amount of $CHCl_3$. Yield: 30.7% (22.0 mg, 14.9 μmol). Anal. Calcd. for $C_{57}H_{45}Cu_2I_2N_3P_2$ (%): C, 56.35; H, 3.73; N, 3.46. Found (%): C, 56.12; H, 3.60; N, 3.38. IR (KBr cm^{-1}): 3070 m, 3048 m, 3030 w, 3000 w, 1600 vs, 1552 m, 1499 m, 1480 s, 1435 vs, 1406 s, 1322 w, 1220 w, 1184 w, 1155 w, 1094 s, 1069 m, 1028 w, 1011 w, 994 w, 840 m, 815 vs, 743 vs, 694 vs, 627 s, 618 s, 523 s, 510 s, 486 m.

Synthesis of $[Cu_2I_2(3\text{-tpyb})_2(PPh_3)_2]_n$ (Cu-3-tpyb)

CuI (19.1 mg, 100 μmol) was added to the THF solution of PPh_3 (55.2 mg, 210 μmol in 5 mL) and the mixture was stirred for 15 min at 40 °C. The bridging ligand, 3-tpyb (15.2 mg, 48.3 μmol), was added to the reaction mixture of CuI and PPh_3. After stirring for 5 min at room temperature, the insoluble impurities were removed by filtration. After standing the filtrate for several days at 30 °C, the pale-yellow crystals were collected by filtration and washed using a small amount of THF. Yield: 29.5% (19.0 mg, 15.7 μmol). Anal. Calcd. for $C_{61}H_{53}Cu_2I_2N_3OP_2$ (%): C, 56.93; H, 4.15; N, 3.27. Found (%): C, 56.70; H, 4.30; N, 3.12. IR (KBr cm^{-1}): 3052 m, 2974 m, 2857 m, 1711 w, 1602 m, 1586 w, 1572 m, 1482 vs, 1436 vs, 1418 m, 1389 m, 1325 m, 1191 m, 1160 w, 1130 w, 1110 w, 1095 s, 1066 m, 1047 w, 1027 m, 1011 w, 997 w, 881 w, 800 m, 747 vs, 695 vs, 512 s, 500 s, 495 s.

Measurements

Elemental analysis of each complex was conducted at the Analysis Center of Hokkaido University, Japan. IR spectra were recorded on a JASCO FT/IR-4100 spectrophotometer as KBr pellets. Emission and excitation spectra were measured by using JASCO FP-8600 spectrofluorometer. UV−Vis diffuse-reflectance and absorption spectra were recorded on a Shimadzu UV-2400PC spectrophotometer equipped with an integrating sphere apparatus. UV-vis diffuse-reflectance spectra were converted to absorption spectra using the Kubelka−Munk function $F(R_\infty)$. Emission quantum yields were measured on a Hamamatsu C9920-02 absolute photoluminescence quantum yield measurement system equipped with an integrating sphere apparatus and a 150 W CW xenon light source. Emission lifetimes and time-resolved emission spectra were assessed using the Hamamatsu Photonics C4334 system, equipped with a streak camera as a photodetector and a nitrogen laser as an excitation light source (λ_{ex} = 337 nm). A liquid-nitrogen cryostat (Oxford Optistat-DN and ITC- 503 temperature controllers) was used to control the sample temperature. PXRD was conducted using a Bruker D8 Advance diffractometer equipped with a graphite monochromator using Cu Kα radiation and a one-dimensional LinxEye detector. Thermogravimetric and differential thermal analysis (TG-DTA) were conducted using a Rigaku ThermoEvo TG8120 analyzer. Single-crystal X-ray diffraction measurements at 150 K were performed using a Rigaku Mercury CCD diffractometer with graphite monochromated Mo Kα radiation (λ = 0.71075 Å) and a rotating anode generator. Low temperature single-crystal X-ray diffraction experiment at 97 K was conducted by using Rigaku XtaLAB Synergy diffractometer with Cu Kα radiation (PhotonJet(Cu)). Each crystal was mounted on a loop using paraffin oil. Diffraction data at 150 K were corrected and processed using Crystalclear.[50] The data at 97 K were corrected and processed using CrysAlisPRO software.[51] The structures at 150 and 97 K were determined by direct methods using SHELXS2013 and SHELXT, respectively.[52] All structure refinements were conducted by the full-matrix least-squares method using SHELXL.[50] All nonhydrogen atoms were refined anisotropically, while hydrogen atoms were refined using the riding model. CrystalStructure[53] and Olex2[54] were used for all calculations for the data at 150 and 97 K, respectively. Crystallographic data for **Cu-4-tpyb** and **Cu-3-tpyb** are summarized in Table S1. Full crystallographic data have been deposited with the Cambridge Crystallographic Data Centre (CCDC 1843260, 1843261, 1852147)

Theoretical calculations

All density-functional-theory (DFT) calculations were performed using the Gaussian 09W program.[55] Geometry optimization of $[Cu_2I_2(PPh_3)_2(m\text{-}pyb)_2]$ was achieved using the Becke3LYP functional[56,57] as implemented in the Gaussian09 program. Cartesian coordinates of the optimized structures are given in Table S3. The SDD basis sets[58,59] and the associated effective core potentials were used for Cu and I, and the 6-31G(d) basis sets[60-61] were used for the remaining atoms.

Acknowledgements

This study was supported by the Shimadzu Science Foundation, the Shorai Science and Technology Foundation, the Murata Science Foundation, Grant-in-Aid for Scientific Research (C)(26410063), Artificial Photosynthesis (Area No. 2406, No.15H00858), and Soft Crystals (Area No. 2903, No. JP17H06367) from MEXT, Japan.

Keywords: Mechanochromism • Delayed fluorescence • Phosphorescence • Luminescence • Cu(I) complex

[1] C. Kutal, *Coord. Chem. Rev.* **1990**, *99*, 213–252.
[2] A. Barbieri, G. Accorsi, N. Armaroli, *Chem. Commun.* **2008**, 2185–2193.
[3] M. Wallesch, D. Volz, D. M. Zink, U. Schepers, M. Nieger, T. Baumann, S. Bräse, *Chem. Eur. J.* **2014**, *20*, 6578–6590.
[4] V. W.-W. Yam, V. K.-M. Au, S. Y.-L. Leung, *Chem. Rev.* **2015**, *115*, 7589–7728.
[5] E. Cariati, E. Lucenti, C. Botta, U. Giovanella, D. Marinotto, S. Righetto, *Coord. Chem. Rev.* **2015**, *306*, 566–614.
[6] K. Tsuge, Y. Chishina, H. Hashiguchi, Y. Sasaki, M. Kato, S. Ishizaka, N. Kitamura, *Coord. Chem. Rev.* **2016**, *306*, 636–651.
[7] A. Kobayashi, M. Kato, *Chem. Lett.* **2017**, *46*, 154–162.
[8] R. Czerwieniec, J. Yu, H. Yersin, *Inorg. Chem.* **2011**, *50*, 8293–8301.
[9] H. Ohara, A. Kobayashi, M. Kato, *Dalton Trans.* **2014**, *43*, 17317–17323.
[10] G. Blasse, D. R. McMillin, *Chem. Phys. Lett.* **1980**, *70*, 1–3.
[11] C. E. A. Palmer, D. R. McMillin, *Inorg. Chem.* **1987**, *23*, 3837–3840.
[12] A. Tsuboyama, K. Kuge, M. Furugori, S. Okada, M. Hoshino, K. Ueno, *Inorg. Chem.* **2007**, *46*, 1992−2001.
[13] M. J. Leitl, F.-R. Küchle, H. A. Mayer, H. Wesemann, H. Yersin, *J. Phys. Chem. A* **2013**, *117*, 11823–11836.
[14] M. J. Leitl, V. A. Krylova, P. I. Djurovich, M. E. Thompson, H. Yersin, *J. Am. Chem. Soc.* **2014**, *136*, 16032–16038.
[15] T. Hofbeck, U. Monkowius, H. Yersin, *J. Am. Chem. Soc.* **2015**, *137*, 399–404.
[16] F. Zhang, Y. Guan, X. Chen, S. Wang, D. Liang, Y. Feng, S. Chen, S. Li, Z. Li, F. Zhang, C. Lu, G. Cao, B. Zhai, *Inorg. Chem.* **2017**, *56*, 3742–3753.
[17] K. R. Kyle, J. A. DiBenedetto, P. C. Ford, *J. Chem. Soc., Chem. Commun.* **1989**, 714–715.
[18] K. R. Kyle, C. K. Ryu, J. A. DiBenedetto, P. C. Ford, *J. Am. Chem. Soc.* **1991**, *113*, 2954–2965.
[19] E. Cariati, J. Bourassa, P. C. Ford, *Chem. Commun.* **1998**, 1623–1624.
[20] H. Kitagawa, Y. Ozawa, K. Toriumi, *Chem. Commun.* **2010**, *46*, 6302–6304.
[21] S. Perruchas, X. F. Le Goff, S. Maron, I. Maurin, F. Guillen, A. Garcia, T. Gacoin, J.-P. Boilot, *J. Am. Chem. Soc.* **2010**, *132*, 10967–10969.
[22] S. Perruchas, C. Tard, X. F. Le Goff, A. Fargues, A. Garcia, S. Kahlal, J.-Y. Saillard, T. Gacoin, J.-P. Boilot, *Inorg. Chem.* **2011**, *50*, 10682–10692.
[23] A. Kobayashi, K. Komatsu, H. Ohara, W. Kamada, Y. Chishina, K. Tsuge, H.-C. Chang, M. Kato, *Inorg. Chem.* **2013**, *52*, 13188–13198.
[24] S.-Z. Zhan, M. Li, S. W. Ng, D. Li, *Chem. Eur. J.* **2013**, *19*, 10217–10225.
[25] X.-C. Shan, F.-L. Jiang, L. Chen, M.-Y. Wu, J. Pan, X.-Y. Wan, M.-C. Hong, *J. Mat. Chem. C* **2013**, *1*, 4339–4349.
[26] T. Hayashi, A. Kobayashi, H. Ohara, M. Yoshida, T. Mastumoto, H.-C. Chang, M. Kato, *Inorg. Chem.* **2015**, *54*, 8905–8913.
[27] F. Farinella, L. Maini, P. P. Mazzeo, V. Fattori, F. Monti, D. Braga, *Dalton Trans.* **2016**, *45*, 17939−17947.
[28] H. Park, E. Kwon, H. Chiang, H. Im, K. Y. Lee, J. Kim, T. H. Kim, *Inorg. Chem.* **2017**, *56*, 8287–8294.
[29] D. V. Scaltrito, D. W. Thompson, J. A. O'Callaghan, G. J. Meyer, *Coord. Chem. Rev.* **2000**, *208*, 243–266.
[30] N. Armaroli, *Chem. Soc. Rev.* **2001**, *30*, 112–124.
[31] D. Felder, J.-F. Nierengarten, F. Barigelletti, B. Ventura, N. Armaroli, *J. Am. Chem. Soc.* **2001**, *123*, 6291–6299.
[32] D. G. Cuttell, S.-M. Kuang, P. E. Fanwick, D. R. McMillin, R. A. Walton, *J. Am. Chem. Soc.* **2002**, *124*, 6–7.
[33] Z. A. Siddique, Y. Yamamoto, T. Ohno, K. Nozaki, *Inorg. Chem.* **2003**, *42*, 6366–6378.
[34] T. McCormick, W.-L. Jia, S. Wang, *Inorg. Chem.* **2006**, *45*, 147–155.
[35] C. E. McCusker, F. N. Castellano, *Inorg. Chem.* **2013**, *52*, 8114–8120.
[36] A. Kobayashi, R. Arata, T. Ogawa, M. Yoshida, M. Kato, *Inorg. Chem.* **2017**, *56*, 4280–4288.
[37] D. Kakizoe, M. Nishikawa, Y. Fujii, T. Tsubomura, *Dalton Trans.* **2017**, *46*, 14804–14811.
[38] M. Mohankumar, M. Holler, E. Meichsner, J.-F. Nierengarten, F. Niess, J.-P. Sauvage, B. Delavaux-Nicot, E. Leoni, F. Monti, J. M. Malicka, M. Cocchi, E. Bandini, N. Armaroli, *J. Am. Chem. Soc.* **2018**, *140*, 2336–2347.
[39] H. Araki, K. Tsuge, Y. Sasaki, S. Ishizaka, N. Kitamura, *Inorg. Chem.* **2005**, *44*, 9667–9675.
[40] H. Ohara, A. Kobayashi, M. Kato, *C. R. Chemie*, **2015**, 1*8,* 766–775.
[41] Y. Okano, H. Ohara, A. Kobayashi, M. Yoshida, M. Kato, *Inorg. Chem.* **2016**, *55*, 5227–5236.
[42] P. C. Ford, E. Cariati, *Chem. Rev.* **1999**, *99*, 3625–3647.
[43] F. Sabin, C. K. Ryu, P. C. Ford, A. Vogler, *Inorg. Chem.* **1992**, *31*, 1941–1945.
[44] B. K. Maiti, K. Pal, S. Sarkar, *Eur. J. Inorg. Chem.* **2007**, 5548–5555.
[45] K. Shimada, A. Kobayashi, Y. Ono, H. Ohara, T. Hasegawa, T. Taketsugu, E. Sakuda, S. Akagi, N. Kitamura, M. Kato, *J. Phys. Chem. C* **2016**, *120*, 16002–16011.
[46] M. Schmittel, B. He, P. Mal, *Org, Lett.* **2008**, *10*, 2513–2516.
[47] A. Pun, D. A. Hanifi, G. Kiel, E. O'Brien, Y. Liu, *Angew. Chem. Int. Ed.* **2012**, *51*, 13119–13122.
[48] H. Yersin, A. F. Rausch, R. Czerwieniec, T. Hofbeck, T. Fischer, *Coord. Chem. Rev*. **2011**, *255*, 2622–2652.
[49] S. Shibata, K. Tsuge, Y. Sasaki, S. Ishizaka, N. Kitamura, *Inorg. Chem.* **2015**, *54*, 9733–9739.
[50] *CrystalClear*; Molecular Structure Corporation: Orem, UT, **2001**.
[51] CrysAlisPro, version 1.171.39.45h; Rigaku Corporation, Oxford, UK, **2018**.
[52] *SHELX*: G. M. Sheldrick, *Acta Crystallogr.* **2008**, A*64*, 112.
[53] *CrystalStructure 4.1*, Crystal Structure Analysis Package; Rigaku Corporation: Tokyo, **2000–2014**.
[54] *Olex2*: O. V. Dolomanov, L. J. Bourhis, R. J. Gildea, J. A. K. Howard, H. Pushmann, *J. Appl. Cryst.* **2009**, *42*, 339.
[55] *Gaussian 09, Revision E.01*, M. J. Frisch, G. W. Trucks, H. B. Schlegel, G. E. Scuseria, M. A. Robb, J. R. Cheeseman, G. Scalmani, V. Barone, B. Mennucci, G. A. Petersson, H. Nakatsuji, M. Caricato, X. Li, H. P. Hratchian, A. F. Izmaylov, J. Bloino, G. Zheng, J. L. Sonnenberg, M. Hada, M. Ehara, K. Toyota, R. Fukuda, J. Hasegawa, M. Ishida, T. Nakajima, Y. Honda, O. Kitao, H. Nakai, T. Vreven, J. A. Montgomery, Jr., J. E. Peralta, F. Ogliaro, M. Bearpark, J. J. Heyd, E. Brothers, K. N. Kudin, V. N. Staroverov, R. Kobayashi, J. Normand, K. Raghavachari, A. Rendell, J. C. Burant, S. S. Iyengar, J. Tomasi, M. Cossi, N. Rega, J.

M. Millam, M. Klene, J. E. Knox, J. B. Cross, V. Bakken, C. Adamo, J. Jaramillo, R. Gomperts, R. E. Stratmann, O. Yazyev, A. J. Austin, R. Cammi, C. Pomelli, J. W. Ochterski, R. L. Martin, K. Morokuma, V. G. Zakrzewski, G. A. Voth, P. Salvador, J. J. Dannenberg, S. Dapprich, A. D. Daniels, Ö. Farkas, J. B. Foresman, J. V. Ortiz, J. Cioslowski, D. J. Fox, Gaussian, Inc., Wallingford CT, **2009**.

[56] A. D. Becke, *J. Chem. Phys.* **1993**, *98*, 5648–5652.

[57] C. Lee, W. Yang, R. G. Parr, *Phys. Rev. B: Condens. Matter Mater. Phys.* **1988**, *37*, 785–789.

[58] W. J. Hehre, R. Ditchfield, J. A. Pople, *J. Chem. Phys*. **1972**, *56*, 2257−2261.

[59] M. M. Francl, W. J. Petro, W. J. Hehre, J. S. Binkley, M. S. Gordon, D. J. Defrees, J. A. Pople, *J. Chem. Phys*. **1982**, *77*, 3654−3665.

[60] D. Andrae, U. Haussermann, M. Dolg, H. Stoll, H. Preuss, *Theor. Chem. Acta*. **1990**, *77*, 123−141.

[61] W. Küechle, M. Dolg, H. Stoll, H. Preuss, *J. Chem. Phys*. **1994**, *100*, 7535−7542.

Entry for the Table of Contents

Layout 1:

FULL PAPER

Unique mechanochromic switching between thermally activated delayed fluorescence and phosphorescence of newly synthesized luminescent Cu(I) coordination polymers, $[Cu_2I_2(PPh_3)_2(m\text{-tpyb})]_n$ (PPh_3 = triphenylphosphine, *m*-tpyb = 1,3,5-tris(*m*-pyridyl)benzene; *m* = 3, 4) has been described.

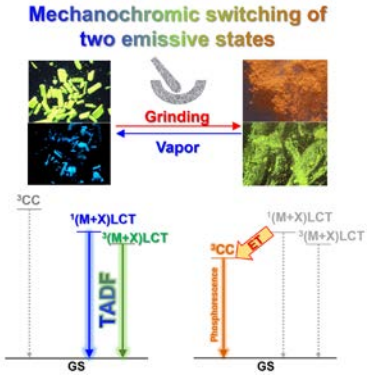

Atsushi Kobayashi, Yuya Yoshida, Masaki Yoshida, and Masako Kato**

Page No. – Page No.

Mechanochromic Switching between Delayed Fluorescence and Phosphorescence of Luminescent Coordination Polymers Composed of Dinuclear Copper(I) Iodide Rhombic Cores